Three-Dimensional EIT Imaging of Breast Tissues: System Design and Clinical Testing

Vladimir A. Cherepenin, *Member, IEEE*, Alexander Y. Karpov, Alexander V. Korjenevsky*, *Member, IEEE*, Vladimir N. Kornienko, Yury S. Kultiasov, Mikhail B. Ochapkin, Olga V. Trochanova, and J. David Meister, *Member, IEEE*

***Abstract*—Results of development and testing of the new medical imaging system are described. The system uses a planar array consisting of 256 electrodes and enables obtaining images of the three-dimensional conductivity distribution in regions below the skin's surface up to several centimeters deep. The developed measuring system and image reconstruction algorithm can be used for breast tissue imaging and diagnostics, in particular for malignant tumor detection. Examples of tomographic images obtained *in vivo* during clinical tests are presented. The mammary gland, being an organ-target, alters at the background with such physiological events as menstrual cycle, pregnancy, lactation, and postmenopause. The objectives of this paper include estimation of the possibilities of electrical impedance mammography for investigation of mammary glands' state among women with different hormonal status. We found that electrical impedance mammograms from different groups had clear visual distinctions and statistically significant differences in mammary glands' conductivity. Our data on conductivity distribution in the mammary gland during different physiological periods will allow us to use it as normal values in the future, to continue this research on mammary glands with different pathology.**

***Index Terms*—Breast tissue diagnostics, electrical impedance tomography, three-dimensional imaging.**

I. Introduction

THE application of nonionizing fields and radiation for breast diagnostics aimed at early tumor detection is a task of current interest for biomedical electronics research. Electrical properties of many tumors and in particular the malignant tumors of the mammary gland significantly differ from the properties of surrounding sound tissues. This fact can be used for the detection and localization of such tumors [1], [2]. The use of electrical impedance tomography (EIT) is a promising application for such detection. Its main advantages include: 1) absolute safety of examination; 2) high potential for significant correlation of biological tissues electrical impedance with their physiological state; 3) compact and inexpensive equipment; and 4) simple examination procedure. Disadvantages of the method are low resolution which falls significantly with increased distance beneath the patient's body surface, as well as the fact that in many instances only so-called dynamic imaging can be fulfilled (i.e., the reconstruction of images of a conductivity change between two consequent measurements). The application of EIT in mammography requires special designs of the measuring system and image reconstruction algorithm. Although there are research projects using common two-dimensional (2-D) EIT with electrodes arranged in a ring [3], we consider the imaging of a three-dimensional (3-D) distribution of conductivity essential to breast diagnostics. This requires applying a 2-D array of electrodes for data acquisition and corresponding reconstruction software, such as suggested in [4], to provide a 3-D image reconstruction.

We have developed a measuring system and image reconstruction algorithm that enables imaging the spatial distribution of conductivity of the medium contiguous to the surface by using a set of electrodes in the form of a planar array on the surface. The visual result is several cross sections of the medium, which are parallel to the electrode array and located at different depths. The paper describes a new measuring system where we have realized some ideas, which appeared after the first model of electrical impedance mammograph as described in [5] had been clinically tested. The preliminary tests of the device demonstrated reproducibility and potential clinical value of images being obtained.

Mammary tissue is an important part of the reproductive system of the female organizm; its tissues are targets for the active effect of sexual steroid hormones, hormones of hypophysis, and other endocrine glands. During such physiological events as menstrual cycle, pregnancy, lactation, and menopause, mammary glands are affected by sexual hormones according to the type of secretion. Nowadays, ultrasound is sometimes used for definition of hormone-dependent changes in breast tissue.

Earlier we have demonstrated that EIT gives the opportunity to obtain an image and digital expression of the mamma's state with cancer [5].

In this research, we tried to estimate possibilities of using EIT in the examination of mammary glands with different hormone's status.

Manuscript received August 30, 2001; revised March 26, 2002. This work was supported by Technology Commercialization International, Inc. *Asterisk indicates correspnding author.*

V. A. Cherepenin is with the Institute of Radio-Engineering and Electronics of Russian Academy of Sciences, Moscow 101999, Russia.

A. Y. Karpov is with the Clinical Hospital No 9, Yaroslavl 150033, Russia.

*A. V. Korjenevsky is with the Institute of Radio-Engineering and Electronics of Russian Academy of Sciences, Mokhovaya 11-7, Moscow 101999, Russia (e-mail: korjenevsky@cplire.ru).

V. N. Kornienko and Y. S. Kultiasov are with the Institute of Radio-Engineering and Electronics of Russian Academy of Sciences, Moscow 101999, Russia.

M. B. Ochapkin and O. V. Trochanova are with the Yaroslavl State Medical Academy, Yaroslavl 150000, Russia.

J. D. Meister is with Technology Commercialization International, Inc., Albuquerque, NM 87110 USA.

Publisher Item Identifier 10.1109/TMI.2002.800602.

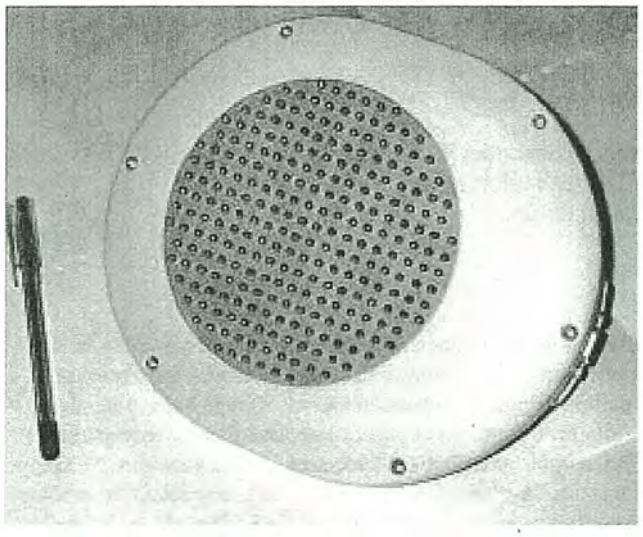

Fig. 1. View of the electrodes array.

II. Materials and Methods

A. Measuring System

The measurements are carried out using a 256-electrode array. The electrodes are arranged in a round matrix with a diameter of 12 cm (Fig. 1). During an examination, the plane of electrodes is pressed against the breast, flattening it toward the chest. This increases the number of electrodes in contact with the breast and decreases the thickness of the tissue layer to be measured. The conversion, from a square array applied in a previous design to a round array, allowed a substantial increase in the electrodes' utilization factor. There are no corner areas in the new system. In such the areas, the electrodes had practically no contact with a patient's skin. Also, the diameter of the array and the number of electrodes being the same, their density increased (the distance between adjacent electrodes became less), this fact has promise for increasing the system's resolution. Two remote electrodes are attached to patient's wrist by means of a clip. The first remote electrode acts as a common current source electrode; the other remote electrode is a potential difference detector reference electrode. Standard extremity electrocardiogram electrodes are used.

The current source consists of a microprocessor controlled digital-to-analog (D/A) converter and a voltage–current converter. A voltage threshold detector connected to the current source output permits the detection of bad contacts with a patient's skin (high contact impedance) and, therefore, improves the image reconstruction process. The criterion of a bad contact is when the output voltage exceeds threshold, which is below the limits of the linearity of the current source. In the case of active load, it corresponds to the resistance exceeding approximately 10 kΩ. During the measurement process, the output 256-channel analog multiplexer switches a single lead from the current source to activate a single electrode in the electrode array. The current source circuit is closed through a patient's body and the grounded remote electrode positioned on a patient's wrist. The current frequency can be changed by means of the embedded software; the maximum operating frequency of the apparatus is 110 kHz. Due to the primary capacitive nature of the skin impedance, it is easier to provide sufficient contact of the electrodes with the body without putting high conductive media on the skin at higher frequencies. On the other hand, the parasitic capacitances limit the accuracy of measurements at high frequency. After the system tests, the operating frequency of 50 kHz has been chosen as optimal because of convenience of measurements (it is possible to make measurements with only slightly moistened skin) and the low level of spurious couplings. The amplitude of rectangular waveform current used in the described measuring system is 0.5 mA.

The potential difference detector consists of an integral instrumentation amplifier with the controlled gain factor, a passive lowpass filter, analog-to-digital (A/D) converter and the embedded software for digital signal processing. During the measuring process, one of the differential inputs of the instrumentation amplifier is switched to a single electrode in the electrode array by means of 256-channel multiplexer. The other amplifier's input is connected to the remote reference electrode positioned on a patient's wrist. The D/A converter output of the contact potential compensation system is connected to the instrumentation amplifier bias input. Before starting measurements on the next electrode, the system measures the contact potential and calculates the code, which is necessary to deliver to this D/A converter for compensation. If the system is not able to compensate the contact potential difference after several attempts, the electrode is marked as faulty in the corresponding table. A 14-bit A/D converter (actual conversion accuracy is 13 bit) is applied in the system. Digital signal detection, device control, and communication with a host computer are carried out by means of the embedded single-chip microcontroller (Atmel's AT90S8515).

The sequence of measuring system operation is the following. The potential difference detector is switched by the multiplexer to the first array electrode, the procedure of contact potential difference compensation is carried out, after that the current source successively switches to each of the remaining electrodes of the array and measurements are fulfilled. The instrumentation amplifier's gain factor is adjusted depending on the distance between the injecting and the measuring electrodes for maximum utilization of A/D converter's dynamic range. After that the cycle is repeated to measure another electrode. A switch-over of the measuring electrode in the external (slow) cycle decreases influence of transients, related with contact potential jumps on the detector's input. A whole data set used for 3-D conductivity reconstruction consists of 65 280 results of measurements. Data processing and measurement process initiating are carried out by means of a personal computer connected to the device by RS-232 communication channel with a 115 200 bit/s rate. Data transmission and measurement processing are being implemented simultaneously, thus, a full measurement cycle takes less than 20 s.

B. Image Reconstruction

The method of backprojection along hemispherical equipotential surfaces of the electric field is applied for 3-D conductivity reconstruction in a medium near the electrodes array. The 3-D imaging allows improved localization of findings without carrying out multiple investigations. In particular,

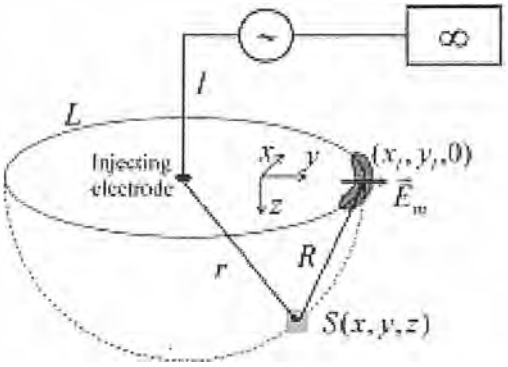

Fig. 2. Reconstruction of 3-D distribution of conductivity.

it gives information regarding the depth of the detected abnormalities and decreases the masking of deeper objects. The key elements of the algorithm have been described in [5]. In addition, it should be mentioned that the array form has been changed from square to round allowing a slight correction of the projecting procedure. Besides, the weight coefficients applied in projecting have been optimized to equalize the tomographic system's sensitivity in depth. While the reconstruction algorithm provides static imaging, it does not provide the absolute values of conductivity, and reconstructed conductivity is presented in arbitrary units. The conductivity value S in the point (x, y, z) is calculated according to

$$S(x,y,z) = 1 + W_1(z) \sum_i \frac{1}{\int\limits_{L(x,y,i)} W_2(l)dl} \times \int\limits_{L(x,y,i)} \frac{W_2(l)(E_r(l) - E_m(l))}{E_r(l)} dl$$

$$W_2 = \frac{1}{R^4} = \frac{1}{((x - x_l)^2 + (y - y_l)^2 + z^2)^2}$$

where W_1 is monotone increasing weight function, which equalizes sensitivity in depth z, i is the number of the injecting electrode, and $L(x, y, i)$ is the line of intersection of the equipotential surface with the plane $z = 0$, on which the electrodes are arranged. The components of the measured electric field vector $\vec{E}_m$ are calculated at the nodes of the grid between the electrodes as the potential differences between adjacent electrodes in the x and y directions. Then these components are linearly interpolated to the current point of integration on the line L. The reference intensity of the electric field E_r corresponds to a homogeneous medium and is calculated numerically. See Fig. 2 for detailed definitions of geometrical values used in the equation.

The reconstruction results in electrical impedance images of seven cross-sectional slices of the investigated medium parallel to the electrodes' plane each with an 8-mm depth step starting at 4 mm from the surface (see Fig. 3). The size of each image (from left to right and from bottom to top) represents the diameter of the electrodes array (12 cm). There are several tools for additional processing of obtained images. To increase contrast or to make some parts of an image more distinct, it is possible to change or adjust the gray scale applied for conductivity

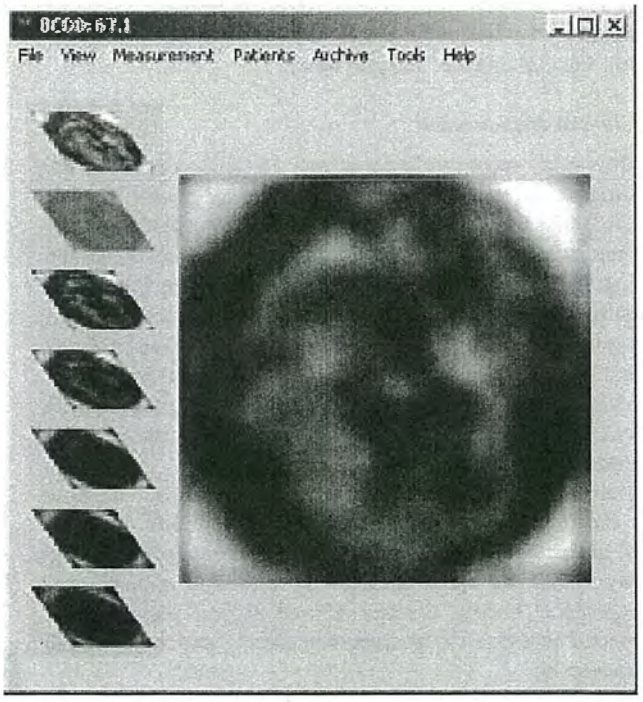

Fig. 3. EIT cross sections.

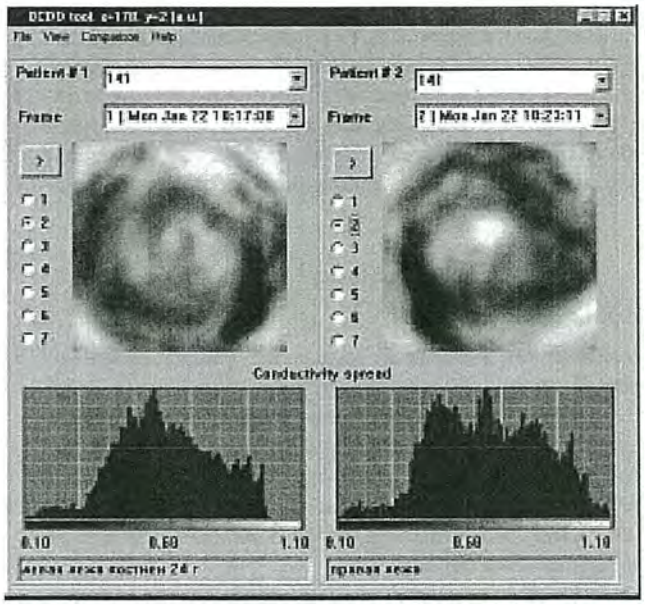

Fig. 4. Comparison of images and histograms of normal breast (left) and breast with tumor (right) of the same patient (aged 70, 24 years in menopause).

imaging. It is also possible to compare two images, e.g., images of left and right breasts both visually and using frequency diagrams of image brightness distribution (histograms); see illustration in Fig. 4. To the latter case, the Kolmogorov–Smirnov nonparametric statistical criterion can be applie to determine the difference between histogram under estimation and, e.g., a histogram of standard image considered to be a nom. There is also a possibility of creating images that look similar to the images

produced by the T-Scan [2] system, i.e., without depth differentiation. We call this the "integral view."

C. Clinical Measurement

Fifty-seven women-volunteers from 18 to 61 years old were investigated. They were divided on five clinical groups: the first group consisting of 12 women from 18 to 45 years old at the first menstrual cycle phase (from 1 to 10 days); the second group consisting of 12 women from 18 to 45 years old at the second menstrual cycle phase (from 16 to 28 day); the third group consisting of 14 women from 18 to 39 years at pregnancy (37–40 weeks); the foutth group consisting of 14 women from 18 to 39 years at lactation period (3–5 days after labor); and the fifth group consisting of five women from 47 to 61 years at postmenopause (more than one year).

Criteria for choosing woman-volunteers for investigation were the following: absence of patient's complaints on mammary glands, absence of mammary gland diseases, normal 28-day menstrual cycle, absence of alarming somatic and gynecological history, absence of pathological alterations at ultrasound investigation of mammary glands, and no hormonal contraception.

The breast scans were made in supine and standing positions. Duration of one patient investigation (electrodes application, mammogram registration, image processing) was about 10–15 min.

The analysis of obtained electrical impedance mammograms (EIM) included: visual image estimation, evaluation of general parameters of conductivity and its variability (mean value, standard deviation, and maximum and minimum values); varying statistical methods (Students criteria); comparison of conductivity values obtained during investigation at different frequencies.

III. Results

A. Laboratory Tests

To estimate and optimize the instrument's parameters, the tomographic system has been tested by means of a dielectric tank filled with water with test objects immersed. Examples of such imaging are demonstrated on the Figs. 5 and 6. On Fig. 5 the images of cross sections of the glass (tube with bottom) immersed in the tank are shown. Fig. 6 demonstrates the view of a small ball made from aluminum foil, which is placed in the tank at some distance from the device.

Due to the primary capacitive nature of the skin impedance, it is easier to provide sufficient contact of the electrodes with the body without putting high conductive media on the skin at higher frequencies. On the other hand, the parasitic capacitances limit the accuracy of measurements at high frequency. The tank tests have demonstrated that the visualization quality (resolution and sensitivity) remains stable at frequencies up to 60 kHz. For higher frequencies, the influence of artifacts became apparent.

Increasing averaging time during measurements has no influence on the visualization results. This fact indicates that image degradation at higher frequencies is due to systematic errors, probably related with spurious couplings arising from the crosstalk and stray capacitances in the multiplexers and other input circuits of the measuring system. The working frequency of 50 kHz was considered optimal and was used in further clinical investigations.

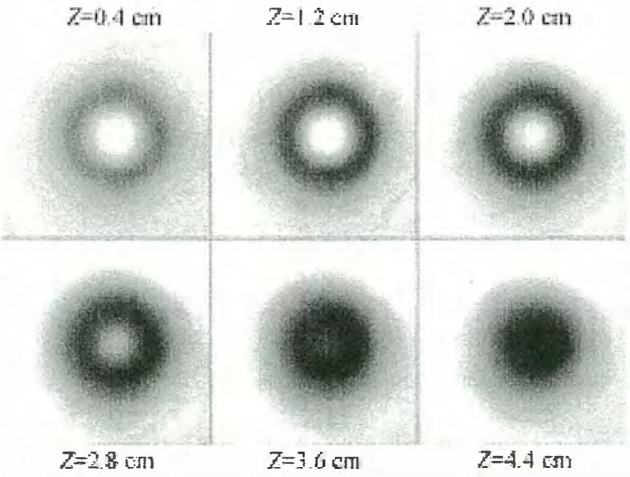

Fig. 5. Tank imaging: the glass (tube with bottom) is immersed to the water vertically, diameter of the glass is 5 cm, height is 9 cm, distance from the electrodes is 1 cm; Z is depth from the electrodes.

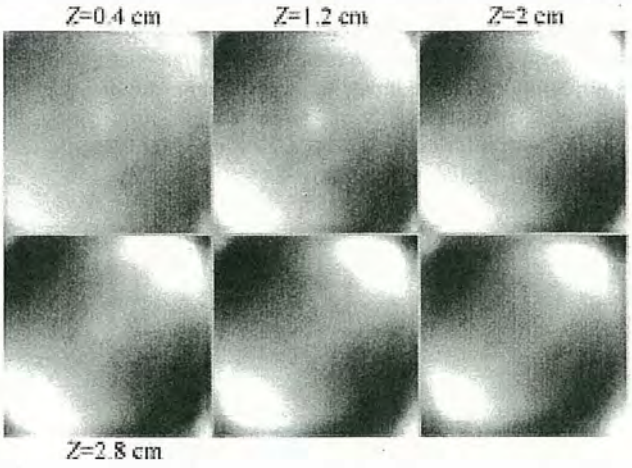

Fig. 6. Tank imaging: the ball from aluminum foil (white spot near the center), diameter of the ball is 0.8 cm, distance from the electrodes is 2 cm; Z is depth from the electrodes.

B. Clinical Results

During the first clinical tests, it was established that the system could visualize breast anatomic structures, which are peculiar for every patient, including areas of pathologic changes that appear in images mostly as white spots (increased conductivity). The imaging results have good reproducibility not only for several measurements taken during one examination but also for measurements taken after significant periods of time.

1) EIT Images of Mammary Glands: Electrical impedance images present the mammary gland conductivity in grey scale; change from dark to light corresponds to change from low electric conductivity to high. For correct image estimation, we compared mammograms from the same cross section (scanning plane).

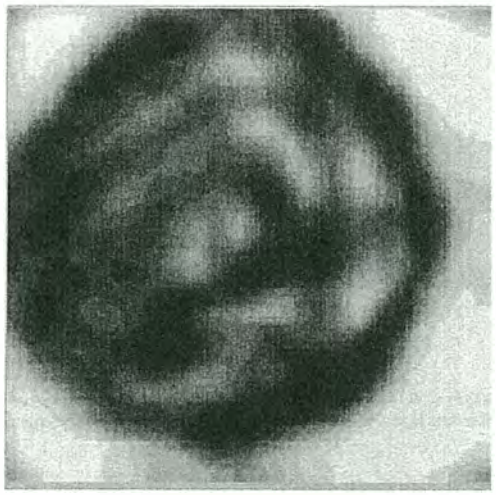

Fig. 7. EIT image of normal breast in the first phase of menstrual cycle (age 22, eighth day in cycle).

Fig. 8. EIT image of normal breast in the second phase of menstrual cycle (age 34, 22nd day in cycle).

Fig. 9. EIT image of breast at pregnancy (age 34, 39th week in pregnancy).

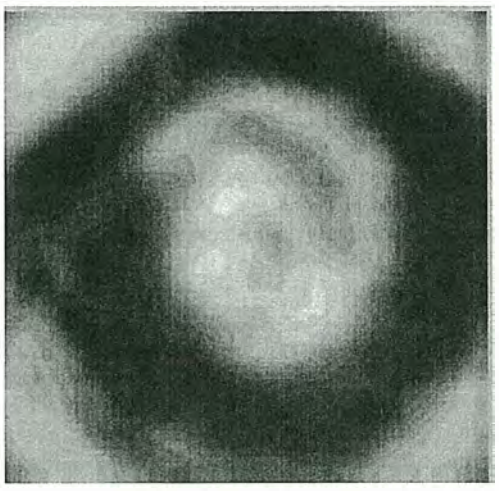

Fig. 10. EIT image of breast at lactation period (age 34, third day after labor).

In the first phase of the menstrual cycle (1–10 days), cell proliferation occurs in the duct-lobe structure under the influence of estrogen. EIM image of mammary gland in the first phase is characterized by smooth allocation of grey tones and absence of symptomatic node (Fig. 7). "Mosaic" structure of images is explained by its complex anatomical composition.

In the second phase (16–28 days), because of estrogen receptors down-regulation in mammary gland epithelium under the influence of a rising quantity of progesterone, the gradual decreasing of cell proliferation begins. Then evolution and differentiation of alveoli and secretory transformation of gland tissue follows. At the end of the first phase, the apoptosis takes place. EIM images of the mammary gland in the second phase (Fig. 8) are also characterized by smooth allocation of grey tones and absence of symptomatic node; moreover there are more light tones as compared with the first phase (Fig. 7). The presence of light tones can be explained by the increased quantity of secrete or liquid in breast tissues because of changes in gland epithelium causing the tissue conductivity to increase.

At pregnancy (37–40 weeks), the combined influence of progesterone, prolactin and estrogens of placenta are accompanying the morpho-functional preparation for lactation. At the end of pregnancy, mamma consists of glandary tissue because of developing lobules, decreased connective tissue and increased volume of ducts. EIM images of the mammary gland at the end of pregnancy are characterized by smooth allocation of grey tones and presence of light tones (Fig. 9).

At the end of pregnancy and during the first days after labor—due to the abrupt decrease of the placenta's estrogen level, there is the prolactin peak ejection, which switches on the lactation mechanism. At lactation, EIM image are characterized by a distribution of dark tones on the periphery and contrasting light tones in the center (Fig. 10). This reflects milk accumulation in the main ducts and increased tissue conductivity.

During postmenopause, when the level of estrogens and gestagens decrease, the replacement of glands by fat, connective tissue, and hyaline tissue starts. EIT image of the mammary gland during menopause looks lighter with contrast changes to dark tones. No symptomatic nodes are present (Fig. 11).

2) Conductivity of Mammary Glands at Different Conditions: For estimation of mammary gland tissue conductivity, we used average values from the second scanning plane (1.2-cm depth). Conductivity is presented in conventional units.

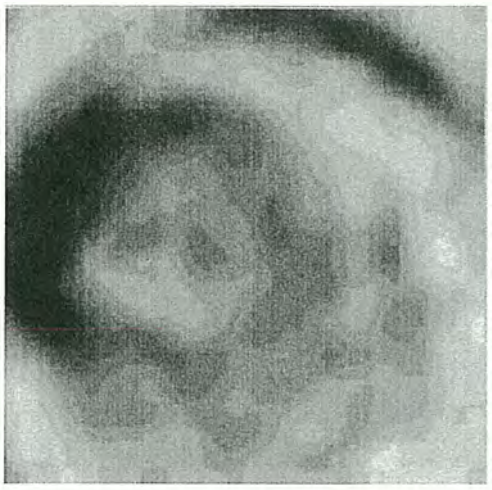

Fig. 11. EIT image of breast at menopause (age 52, three years in menopause).

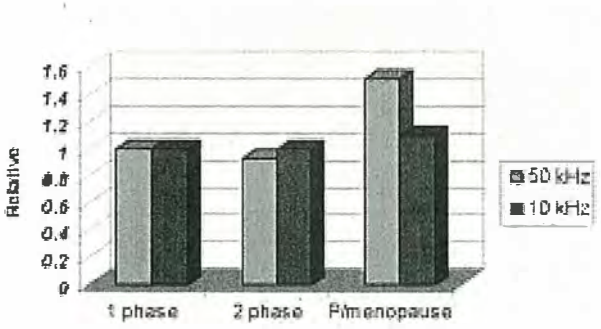

Fig. 12. Changes of mammary conductivity at different frequencies (50 kHz and 10 kHz). The data is normalized to one for the first group at both frequencies.

Conductivity of mamma in the supine position is higher in all groups but we did not find statistically significant differences ($p > 0.05$). In further computations, we used conductivity values measured from supine position.

Tissue conductivity of left and right mammary glands in all groups does not differ ($p > 0.05$).

We did not find statistically significant differences in groups 1, 2, 3, and 4 ($p > 0.05$). There is a difference in conductivity in group 5 relative to groups 1, 2, 3, and 4 ($p < 0.001$).

In this research, we compared results of measurements carried out using a first-generation system operating at 10 kHz with the new system working at 50 kHz, comparing them as current of low and high frequency. Because of different reconstruction algorithms it would be incorrect to compare absolute results of conductivity obtained with different systems. It would be more objective to compare the percent of increase/decrease of mean conductivity of mammary glands of women from different groups at one frequency, to percent increase/decrease of mean conductivity at another frequency. There is an interesting comparison of the percent of increase of mean conductivity of mammas from women from group 1 and 2 to group 5 while using different frequency. While using the 10 kHz current there is an increase in mean conductivity by 11%, but at 50 kHz, the increase in conductivity is 52%– 64% (Fig. 12). It can be explained by the dispersion properties of connective tissue and hyaline stroma developing in mammary glands at postmenopause.

IV. Discussion

The change in form of the electrode array as well as the transition to digital signal processing improved the measuring system characteristics. Also, the device design has been simplified by reducing the number of precision analog components.

The results of clinical tests allow stating that the device, operating at a frequency near 50 kHz, is capable of visualizing the electrical impedance structure of breast tissues and obtaining results that are of clinical value. Stepping up the device operation frequency to 60 kHz or more results in impairment of image quality. This is first of all associated with the spurious capacitances in the measuring system's input circuits.

Two-frequency measurements, for example, at 10 and 50 kHz enable frequency variance estimation of abnormalities found in electrical impedance images that may simplify their identification. Such two-frequency measurements can be realized by means of the measuring system described in the paper.

EIT images of mammary glands seem to be the same at the first and second phases of the menstrual cycle and also at the period of pregnancy. During lactation, light colors at the center of the image reflect increased conductivity due to the milk content in the galactophorous ducts. EIT images at menopause are visually distinguished from the images during fertility.

Conductivity analysis shows that mean conductivity of mamma for a healthy woman in the supine position is higher than in a standing position. It may be related to hemodynamic changes when changing position of the patient. The conductivity of mammary glands in a healthy woman is the same at first and second phase of a 28-day menstrual cycle. The conductivity increase in postmenopausal breasts observed in the experiments can be explained by involution processes. These processes include not only replacing the mammary gland with fat, but also increasing the connective and hyaline tissue.

Our data on conductivity of mamma's tissue in women during different physiological periods allows us to use the information as normal values in the future and continue this research on mammary glands with different pathology.

References

[1] A. J. Surowiec, S. S. Stuchly, J. R. Barr, and A. Swarup, "Dielectric properties of breast carcinoma and the surrounding tissues," *IEEE Trans. Biomed. Eng.*, vol. BME-35, pp. 257–262, 1988.

[2] M. Assenheimer, O. Laver-Moskovitz, D. Malonek, D. Manor, U. Nahaliel, R. Nitzan, and A. Saad, "The T-SCAN TM technology: electrical impedance as a diagnostic tool for breast cancer detection," *Physiol. Meas.*, vol. 22, pp. 1–8, 2001.

[3] A. Hartov, T. E. Kerner, M. T. Markova, K. S. Osterman, and K. D. Paulsen, "Dartmouth's next generation EIS system: preliminary hardware considerations," *Physiol. Meas.*, vol. 22, pp. 25–30, 2001.

[4] J. L. Mueller, D. Isaacson, and J. C. Newell, "A reconstruction algorithm for electrical impedance tomography data collected on rectangular electrode arrays," *IEEE Trans. Biomed. Eng.*, vol. 46, pp. 1379–1386, Nov. 1999.

[5] V. Cherepenin, A. Karpov, A. Korjenevsky, V. Kornienko, A. Mazaletskaya, D. Mazourov, and D. Meister, "A 3D electrical impedance tomography (EIT) system for breast cancer detection," *Physiol. Meas.*, vol. 22, pp. 9–18, 2001.

Diagnostics of dyshormonal mammary gland diseases with multifrequency electrical impedance mammography

O.V. Trokhanova[1], M.B. Okhapkin[1] and A.V. Korjenevsky[2]

[1] Yaroslavl State Medical Academy, Yaroslavl, Russia
[2] Institute of Radio-engineering and Electronics of the RAS, Moscow, Russia

Abstract— **More than 34 000 new cases of breast cancer are registered annually in Russia with the patients age becoming significantly younger. 25% of women under thirty and 60% of those above forty are diagnosed as dyshormonal mammary glands (mastopathy) cases. Though mastopathy is not considered to be obligatory cancer prelude, breast cancer occurs 3 - 5 times more often in patients with diffuse dyshormonal non-cancerous diseases of mammary glands and 30 - 40 times more often with nodular forms of mastopathy aggravated by proliferation of lactic gland epithelium [1]. This evidence has heightened the general interest in non-malignant growth opening the way to incidence reduction in breast cancer through effective curing of mastopathy. The existing methods of mastopathy diagnosis have certain applicability restrictions of both objective and subjective nature. The report presents main results of a comprehensive examination of 166 women (92 without breast pathology and 74 with mastopathy) with four methods: multifrequency electrical impedance mammography, ultrasonic investigation, x-ray mammography and puncture biopsy. The analysis of the obtained data was based on visual estimation of the electrical impedance images, estimation of indices and histograms of the conductivity distribution in mammary glands under multifrequency investigation, comparison of measurements in different groups according to Student's criterion and comparison with ultrasonic and x-ray data. The report presents criteria of diagnostics of various forms of mastopathy using the multifrequency electrical impedance mammography method.**

Keywords— **medical application of EIT, EIT diagnostics of mammary gland, multifrequency EIT, breast cancer, mastopathy.**

I. Introduction

The aim of the investigation is to estimate possibilities of multifrequency electrical impedance mammography to diagnose dyshormonal mammary gland diseases.

II. Subjects

The report presents main results of a comprehensive examination of 166 women (92 without breast pathology in the 1st group and 74 patients with mastopathy in the 2nd group). In both groups there were formed special period subgroups according to the degree of age change of mammary glands:

- below 35 years — with normal stable state of mammary glands;
- 35–40 years — with gradual loss of glandular structures;
- 41–45 years — with noticeable thickening of duct cylindrical epithelium, thickening of basal membrane and fibrous change of connective tissue;
- 46–50 years — with dilatation and occasional cystic widening of lactic ducts surrounded by fibrous tissue;
- above 50 years — with slow obliteration of lactic ducts and small vessels accompanied by adipose tissue formation.

III. Methods

The following diagnostic methods were applied:

- ultrasonic examination of mammary glands was applied to all patients on the 5–9th days of their menstrual cycle; the apparatus used was ultrasonic Combison 530 with electronic linear 7.5 MHz probe;
- women of 35 upwards were subjected to x-ray mammography on the 5–9th days of their menstrual cycle; 'Mammodiagnost UC X-ray apparatus and ACFA mammoray HDR film in Kodak min-R cassette were used;

- all patients were subjected to multifrequency electrical impedance mammography; the apparatus used was a 256-electrode electrical impedance mammograph, developed by the Institute of Radio-Engineering and Electronics of the Russian Academy of Science; the frequencies used were 10 kHz and 50 kHz; the timing was chosen 3–10th and 17–28th days of the menstrual cycle;
- after ultrasonic and X-ray examinations, a puncture biopsy was carried out with a puncture needle by standard procedure;
- all examination results were statistically processed by alternative variation method to obtain a mean value and standard deviation. To check the data reliability we resorted to Student's criterion and the appropriate tables. In addition the so called 'least square method' (LSM or Gauss' method) was used from MATLAB 7.0 applications.

IV. Results

All dyshormonal hyperplastic processes in milk glands are known under the term 'mastopathy'. Mastopathy is defined as a fibrous and cystic disease with a wide spectrum of proliferative and regressive changes of the mammary gland with abnormal ratio of epitelic and conjunctive components that are mingled in various combinations.

To find out potentiality of multifrequency electrical impedance mammography in diagnostics of dyshormonal mammary gland diseases, checkups followed the usual procedure of ultrasonic investigation and x-ray mammography (with women of 35 upwards).

92 women with cited below ultrasonic resulting data composed the 1st clinical group [2]:

- ultrasonic type of the mammory glands was in comformity with their age (juvenile, reproductive, premenopausal);
- ultrasonic visualizations corresponded to their physiological periods (1st phase of the menstrual cycle, 2nd phase of the menstrual cycle);
- distinct differentation of the mammary gland tissue;
- the parenchyma thickness did not exceed 14 mm;
- absence of focal symptomatology, ductectasia, duct wall fibrosis;
- absence of changes in regional zones of lymph outflow.

The 2nd clinical group composed 74 women revealing the following ultrasonic information [2]:

- incongruity between ultrasonic type of the mammary glands and their age;
- glandular tissue layer thickening for more than 14 mm in all varieties of diffuse mastopathy;
- fibrous changes in walls of ducts;
- changes in echodensity of glandular tissue indices that they are not typical for the patient's age;
- ductectasia, wall thickening, lumen increase, irregularity of duct circuit, dilations along the main duct;
- presence of multiple cysts.
- Mastopathy women of Group 2 were subdivided into 2 subgroups according to the mastopathy type:
- 1st type mastopathy subgroup — without cyctic component (41 patients);
- 2nd type mastopathy subgroup — with one or numerous cysts (33 patients).

Women of 35 upwards underwent X-ray examination to confirm the diagnosis. Mastopathy patients underwent anticancer and antiatypia puncture thin-needle biopsy.

The analysis of the multifrequency electrical impedance mammography began with consideration of electrical conductivity indices, given in conventional units.

As it was shown in our previous reports there is no statictically valid difference in electrical conductivity indices depending on the vertical or horisontal body position and on the left or right body side [3, 4]. So we thought it safe to use mean indices from the second scanning level. The obtained results are shown in Tables 1 and 2.

The following analysis results should be noted:

- electrical conductivity indices proportionally increase with the patients' age irrespective of their groups and menstruation phases;
- according to the statiscics mastopathy of both types is certain to reduce electrical conductivity from norm in the corresponding age groups of menstruating women (aged up to 50) on frequency 50 kHz as well as 10 kHz during both menstrual cycle phases (in all cases $p<0.05$). As for postmenopause (51–55 years of age), mastopathy does not influence electrical conductivity or has just a slight excess over the norm (disparity is statistically inadequate $p>0.05$).
- in group of the 2nd type mastopathy in all menstruation phases and in postmenopause at the frequency of 50 kHz the electrical conductivity is higher than in mastopathy of the 1st type;
- in norm and mastopathy of the 2nd type, we see a clear, statistically valid decrease in electrical conductivity in both phases of the menstruation cycle and in postmenopause in the corresponding age groups at the frequency of 10 kHz (in all cases $p<0.05$);

- during the 1st type mastopathy the electrical conductivity indices are the same at all frequences and in all groups.

The results of the comparison of the electro impedance images are as follows (Fig.1):

- abnormal architecture of images caused by changes in proportion of mammory gland tissue which results in discrepancy between electro impedance type (juvenile, reproductive, postmenopausal) and the age;
- an increase of hypoimpendance areas owing to fibrose changes of fat tissue, fibrosis duct walls and Kuper's ligament;
- appearance in mastopathy mammograms of the 2nd type hyperimpedance inclusions with clear outline that correspond to the mammary gland cysts or clear widening of the ducts.

Tomogram changes of mammary gland structure are confirmed by the results of ultrasonic examination.

V. Conclusions

From the investigation results we have drawn the following conclusions:

1. Mammary gland electrical conductivity depends on the woman's age irrespective of the presence or absence of structural changes in the gland tissue. To find out the general tendency that is to avoid unimportant, incidental anomalies and abnormalities the experimental data about dependence of electrical conductivity from age were processed according to the "least squares method" (LSM or Gauss's method). The sought for parameters of this dependence were determined. Regression lines in all clinical groups and at the frequency of 50 kHz are described with the same polynomial of degree three ($f(x) = p1 \cdot x^3 + p2 \cdot x^2 + p3 \cdot x + p4$), and the coefficients (p1, p2, p3, p4) of this polynomial are found from the system of linear equations. Norm: 50 kHz (p1=0.0025, p2=-0.01893, p3=0.06857, p4=0.38); 10 kHz (p_1=0.005, p_2=-0.04357, p_3=0.1414, p_4 =0.272). Mastopathy 1 type: 50 kHz (p_1=0.009167, p_2=-0.06464, p_3=0.1662, p_4=0.184); 10 kHz (p_1=0.0075, p_2=-0.05179, p_3=0.1407, p_4=0.188). Mastopathy 2 type: 50 kHz (p1=0.01167, p2=-0.095, p3=0.2733, p4=0.136); 10 kHz (p1=0.01167, p2=-0.1007, p3=0.2876, p4=0.088).
2. In spite of the equal regularity in the changes of the electrical conductivity in norm and during age dysplasia the method of electrical impedance mammography ensures reliable diagnosis of mastopathy by the fall in electrical conductivity indices in the corresponding age groups and at different frequencies in women during menstruation phase. The absence of electrical conductivity difference between norm and mastopathy with women in postmenopause confirms the fact that dysplasia appears due to disfunction in the cystem "ovary — mammary gland" and not as an independent desease.
3. The major advantage of the multifrequency electrical impedance mammography over the monofrequency lies in the fact than it makes it possible not only to diagnose mastopathy but also helps exactly determine cystless form from the absence of difference between indices of mean electrical conductivity in the corresponding age groups during all phases of the menstruation cycle. According to morphologists, occurance rate of hyperplasia and atypia that accompany dysplasia is higher than with cystic form, which makes it possible to ascertain a group of higher risk for special medical care to prevent mammary gland cancer development.
4. Confirmation of visual changes in tomograms during mastopathy by quantitative characteristics of the electro conductivity excludes any diagnostic mistake.
5. Safety of the electrical impedance mammography method makes it possible to use it for screening examination and young women medical supervision.

Table 1 The mean electrical conductivity indices of mammory glands in norm and mastopathy patology in the 1st phase of the menstruation cycle and in the postmenopause with momen of different age groups (10 kHz, 50 kHz). The values are given with deviations.

	19 - 34 years		35 – 39 years		40 – 44 years		45 – 50 years		51 - 55 years Postmenopause	
	50 kHz	10 kHz	50 kHz	10 kHz	50 kHz	10 kHz	50 kHz	10 kHz	50 kHz	10к kHz
Norm	0.43± 0.09	0.37± 0.09	0.47± 0.09	0.44± 0.09	0.47± 0.08	0.41± 0.09	0.52± 0.03	0.48± 0.05	0.56± 0.06	0.51± 0.07
Mastopathy 1 type	0.30± 0.07	0.29± 0.07	0.31± 0.05	0.30± 0.05	0.38± 0.05	0.38± 0.08	0.38± 0.09	0.38± 0.09	0.55± 0.03	0.54± 0.05

Mastopathy 2 type	0.33 ± 0.03	0.29± 0.03	0.38± 0.07	0.34± 0.07	0.44± 0.09	0.38± 0.06	0.44± 0.03	0.36± 0.07	0.59± 0.02	0.47± 0.03

Table 2 The mean electrical conductivity indices of mammory glands in norm and mastopathy patology in the 2nd phase of the menstruation cycle and in the postmenopause with momen of different age groups (10 kHz, 50 kHz). The values are given with deviations.

	19 - 34 years		35 – 39 years		40 – 44 years		45 – 50 years		51 - 55 years Postmenopause	
	50 kHz	10 kHz	50 kHz	10 kHz	50 kHz	10 kHz	50 kHz	10 kHz	50 kHz	10 kHz
Norm	0.43± 0.09	0.39± 0.08	0.48± 0.03	0.43± 0.04	0.48± 0.03	0.43± 0.03	0.53± 0.05	0.48± 0.05	0.56± 0.06	0.51± 0.07
Mastopathy 1 type	0.28± 0.05	0.27± 0.07	0.30± 0.07	0.29± 0.07	0.35± 0.05	0.36± 0.06	0.38± 0.09	0.37± 0.09	0.55± 0.03	0.54± 0.05
Mastopathy 2 type	0.33 ± 0.07	0.29± 0.04	0.36± 0.06	0.31± 0.05	0.4± 0.09	0.34± 0.06	0.46± 0.04	0.37± 0.05	0.59± 0.02	0.47± 0.03

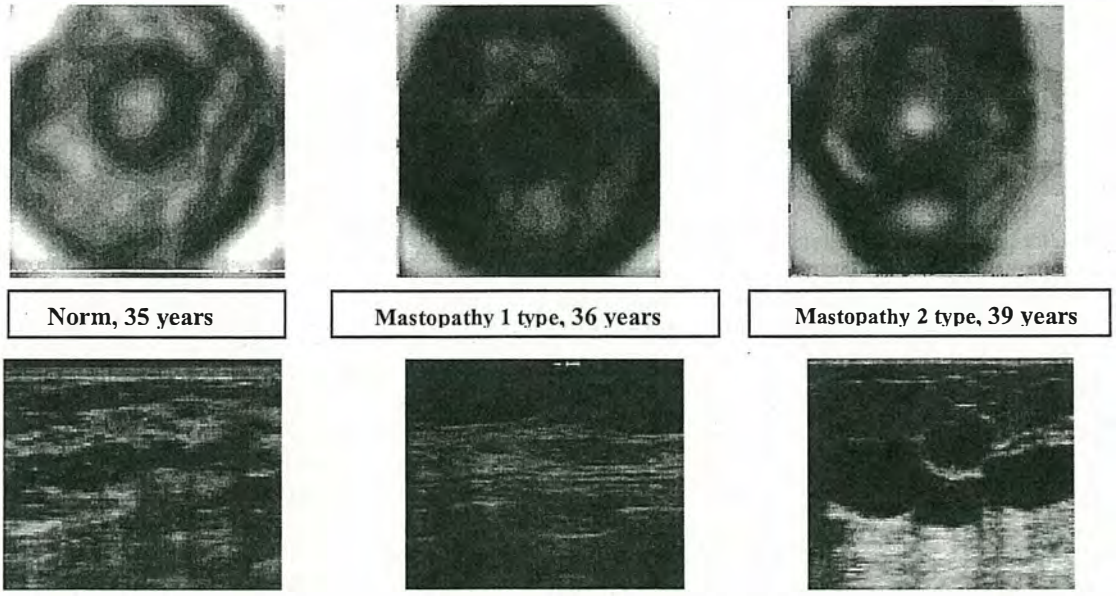

Fig. 1. Electro impedance and ultrasonic images of mammory glands in norm and during mastopathy (the 2nd scanning level, 50 kHz)

References

1. Letyagin V P (2000) Mastopathy. RMM Gynaecology 8:468-472
2. Leucbt W (1992) Teaching. Atlas of breast ultrasound. Thieme Verlag, Stuttgart
3. Cherepenin V A, Karpov A Y, Korjenevsky A V, et al. (2002) Three-Dimensional EIT Imaging of Brest Tissues: System Design and Clinical Testing. IEEE Trans Med Imag 21:662-667
4. Trokhanova O V, Karpov A Y, Ochapkin M B et al. (2001) Electro-impedance mammography testing at some physiological woman's periods. 3rd EPSRC Engineering Network Meeting, London, UK, 2003, pp 134-138

Address of the corresponding author:

Author: Olga Trokhanova
Institute: Yaroslavl State Medical Academy
Street: Voljskaya Naberejnaya, 15
City: Yaroslavl
Country: Russia
Email: trokhanova@[redacted]

INSTITUTE OF PHYSICS PUBLISHING PHYSIOLOGICAL MEASUREMENT

Physiol. Meas. **22** (2001) 9–18 www.iop.org/Journals/pm PII: S0967-3334(01)19980-6

A 3D electrical impedance tomography (EIT) system for breast cancer detection

V Cherepenin[1], A Karpov[2], A Korjenevsky[1], V Kornienko[1], A Mazaletskaya[3], D Mazourov[4] and D Meister[5]

[1] Institute of Radio-Engineering and Electronics of Russian Academy of Sciences, Moscow, Russia
[2] Clinical Hospital No 9, Yaroslavl, Russia
[3] Yaroslavl State University, Russia
[4] Regional Oncological Hospital, Yaroslavl, Russia
[5] Technology Commercialization International, Inc., Albuquerque, NM, USA

E-mail: korjenevsky@[redacted] almaz@[redacted] and tcintl@[redacted]

Received 12 December 2000

Abstract

A medical device which allows imaging of the distribution of conductivity in 3D in regions below the skin surface has been developed and tested. Its purpose is to enable early detection and preliminary diagnosis of breast tumours. Design of the measuring system and software are described. Results of clinical evaluation of the system are presented. EIT images of healthy and cancerous breasts are presented and discussed. The system is able to visualize various states of the breast and it may be possible to apply it to breast cancer detection.

Keywords: electrical impedance tomography, breast cancer detection, bio-impedance, medical imaging

1. Introduction

The electrical conductivity of many tumours, in particular the malignant tumours of the breast, may significantly differ from the conductivity of surrounding normal tissue (Rigaud *et al* 1996). This provides a possible way to provide an efficient, safe and inexpensive method to detect and localize such tumours, using electrical impedance tomography (EIT). This technique enables visualization of the spatial distribution of conductivity in the human body; several research groups work on EIT systems for breast imaging (see, for example, Tunstall *et al* 1998, Wtorek *et al* 1999). Application of this method to breast cancer detection requires special design of the measuring system and image reconstruction algorithm, as imaging of a three-dimensional distribution of conductivity is required. The resolution of the EIT system falls significantly with increasing distance from measuring electrodes, and traditional EIT measurement schemes are unsuitable for mammography because of this. A large number of electrodes, which are required to provide acceptable resolution of the system, leads to enormous increases in computation time for image reconstruction.

The prototype of the breast cancer detection device (BCDD), presented in this paper, which is suitable for carrying out clinical recordings, has been developed in the Institute of the Radio-Engineering and Electronics of the Russian Academy of Sciences with the support of Technology Commercialization International, Inc. (USA). It is a 3D EIT system which consists of a compact array of electrodes positioned over the tissue being measured, two additional electrodes placed remotely from the array of electrodes, a source of alternating (AC) current, a means to measure potential difference and computing means to reconstruct and visualize the conductivity distribution as stack of tomographic images.

A comparative analysis of electrical impedance images obtained with the new system in normal and cancerous breasts is presented in this paper.

2. Materials and methods

2.1. Measuring system

The measurements are carried out using 256 electrodes, which are arranged in a square matrix with sides of 12 cm. The electrodes are supported on a rigid plane, from which each electrode protrudes. During an examination, the plane of electrodes is pressed against the breast, so flattening it toward the chest. This increases the number of electrodes in contact with the breast and decreases the thickness of the tissue layer to be measured. The 3D EIT system includes an output multiplexer, which is connected to the electrode array and is the means by which an alternating current (AC) source is connected to one of the electrodes in the array. An input multiplexer connects one of the remaining electrodes of the array to a potential difference measuring unit. A microprocessor in the 3D EIT system and computer determine through which electrode current is driven and which electrode is selected for potential difference measurement. Two single remote electrodes are attached to the extremities of the patient. One remote electrode is connected directly to a safe AC source (0.2 mA, at 10 kHz, whereas the maximum allowable safe level is 1.0 mA, at 10 kHz). The other remote electrode is connected directly to the potential difference detector. The 3D EIT system operation is controlled by a microprocessor and computer.

The output multiplexer switches a single lead from the AC source to activate a single electrode in the electrode array at a time, instead of activating pairs of electrodes. The second activated electrode is a remote electrode that is always on. The input multiplexer functions in a similar fashion. The potential difference detector measures the difference between the selected array electrode and a remote rest electrode. For a given input electrode, the output multiplexer sequences through all the other electrodes in the array while the potential difference detector makes its measurements. Then the input electrode is switched and the output multiplexer sequence repeated. Switching a single lead at a time reduces the spurious couplings which arise from cross-talk in the multiplexer. It also simplifies the device and reduces its cost. The distance of the remote electrodes from the electrode array supports the assumption that the unperturbed equipotential surfaces of electric field are spherical in the examination area. It simplifies and speeds up the conductivity reconstruction calculations.

The current injection and voltage measurement circuitry is similar to the one in our electrical impedance tomograph for static imaging (Cherepenin *et al* 1995, Korjenevsky *et al* 1997). In the current source, a digital-to-analogue converter provides the input signal for a voltage-to-current converter which consists of three operational amplifiers. In the potential-difference-measuring unit, an analogue synchronous detector and switchable integrator convert input AC potential differences to DC before analogue-to-digital conversion. A synchronous detector provides measurement of the real part of impedance. A 16-bit analogue-to-digital

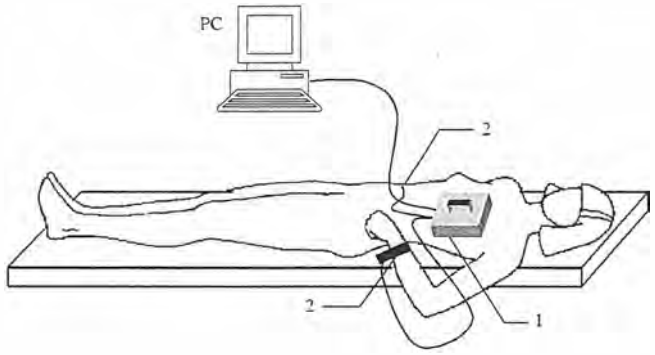

Figure 1. Physical configuration of the system and measuring procedure: 1—plane with 256 electrodes, 2—remote electrodes.

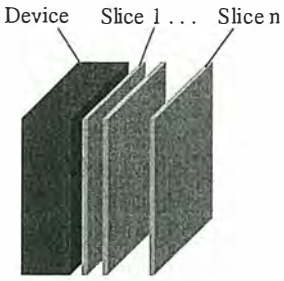

Figure 2. 3D imaging planes.

converter measures voltage. A fast-response circuit for DC potential compensation enables reliable measurements with the stainless steel electrodes that are used. A full measurement cycle (65 280 voltage measurements) takes less than 20 s. Since some of the electrodes on the planar electrode array can be out of contact with patient's body, the measuring system is provided with a voltage threshold detector. This is connected to the current source and checks the quality of contacts. Information from this circuit is used during image reconstruction. Figure 1 illustrates the physical configuration of the system and measurement procedure.

2.2. Reconstruction software

The method of back-projection is one of the fastest in electrical impedance tomography and seems most suitable for 3D applications like this one; for 256 electrodes, the time required for calculations is critical. Our EIT system uses a method of weighted back projection along equipotential surfaces of the electric field to reconstruct the 3D conductivity distribution. It provides visualization of several tomographic cross-sections ('slices'), which are parallel to the electrode array (figure 2).

It is assumed that where the electric current is injected through one of the electrodes in a planar array and the remote common electrode, equipotential surfaces near the array are spherical. The procedure of back projection is reduced to the following. For some point with co-ordinates (x, y, z) inside the object being imaged, the distance is determined between this point and the injecting electrode of the array. This is equal to the radius r of the equipotential

surface containing the point where the conductivity is reconstructed. Knowing this radius, it is possible to determine the line of intersection of the equipotential surface with the surface on which the electrodes are arranged. When the electrodes are arranged on the plane, given by equation $z = 0$, this line is the circle lying in the (x, y) plane having its centre at the point where the injecting electrode is located, and having radius r. Conductivity S (in arbitrary units) at the chosen point is calculated according to the equation

$$S(x, y, z) = 1 + W_1(z) \sum_i \left(\int_{L(x,y,z,i)} W_2(l)\,\mathrm{d}l \right)^{-1} \int_{L(x,y,z,i)} W_2(l)(E_r(l) - E_m(l))/E_r(l)\,\mathrm{d}l$$

where i is the number of the injecting electrode, and $L(x, y, z, i)$ is the line of intersection of the equipotential surface with the surface on which the electrodes are arranged (a circle with radius r). The components of the electric field vector $\vec{E}_m$ are first calculated at the nodes of the grid between the electrodes as the potential differences between adjacent electrodes in the x and y directions. Then these components are linearly interpolated to the current point of integration on the line L and the magnitude of this vector E_m is calculated. The reference intensity of the electric field E_r corresponds to a homogeneous medium and is calculated numerically using the reference data set synthesis technique (Korjenevsky 1995) to improve static imaging. A weighting coefficient $W_1(z)$ corrects the decrease of sensitivity with depth as $W_1 = (z + \alpha)/(z + \beta)$, $\alpha \ll \beta$.

The weighting coefficient W_2 provides a relatively greater contribution to the calculated conductivity of those points on line L, which are located closer to the point at which the conductivity is reconstructed. The 3D EIT system uses the equation $W_2 = 1/R^4 = 1/\left((x - x_l)^2 + (y - y_l)^2 + z^2\right)^2$, where R is the distance between the point where the conductivity is reconstructed and the current point on the line along which integration is being carried out; the index l refers to the coordinates of this point.

Whenever it is difficult to produce sufficient contact of all the electrodes with the patient's body, then the output voltage of the threshold detector is used to determine whether the electrode being used at any particular moment has sufficient contact with the body. The values of the potential differences measured from electrodes that have insufficient body contact cannot be used properly in the process of conductivity reconstruction. Instead, values of potential differences calculated based on a homogeneous conductivity distribution are used.

The resulting electrical impedance image represents tissue conductivity along a grey scale from dark to light, which represents low to high conductivity. The time that is required for the reconstruction of conductivity in seven cross-sectional slices (each with a 8 mm depth step) is less than 1 min with a Pentium II 300 MHz processor.

2.3. Testing of the system in a saline filled tank and the male breast

The device was tested on a saline filled tank and on the male volunteers (the male breast, which is not as complicated as the female breast, was investigated in the first trials). The tank measurements were carried out with the device placed horizontally above the open surface of the saline. The tank, filled with 1% sodium chloride solution, was 10 cm deep and 30×30 cm^2 square. The remote electrodes were placed on the corners at the bottom of the tank. Testing in the tank has demonstrated the accuracy of imaging with test objects up to 5 cm from the planar electrode array (figure 3). A hollow glass cylinder, 5 cm in diameter and 9 cm high (wall thickness 0.5 cm) was immersed vertically in the saline. The distance between the electrodes and top of the test cylinder was approximately 1 cm. In the images, it may be seen that the cylinder appears as a circle at any depth. The structure of the test object appears to simplify

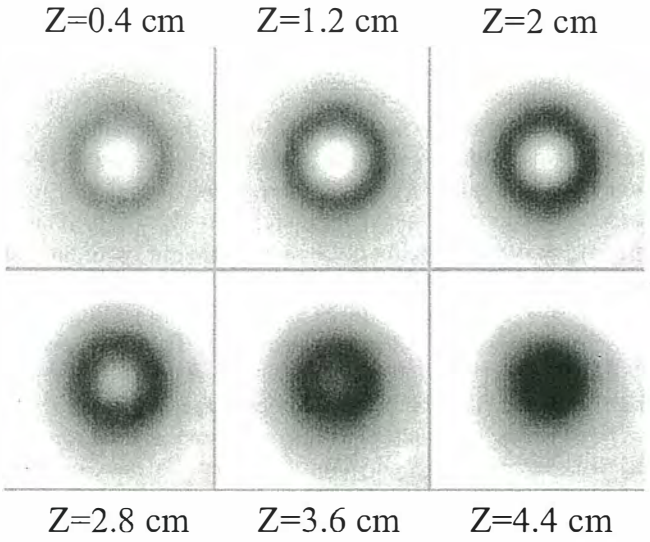

Figure 3. Imaging of a glass cylinder immersed vertically into the saline filled tank.

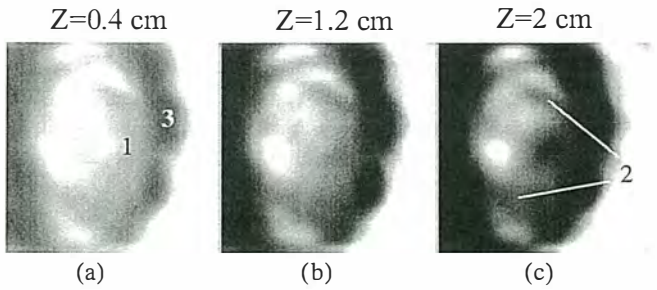

Figure 4. Male breast images at different cross-sections: (a) 0.4 cm, (b) 1.2 cm, (c) 2 cm from the skin surface. Presumed anatomical correlations: 1—nipple, 2—ribs, 3—zone of artefacts, which correspond to the boundary between good and faulty contacts on the electrode plane.

with depth, presumably due to a decrease in device resolution. Other tank measurements were performed with small test objects in order to estimate resolution and sensitivity of the system. In such tests the device clearly imaged an 8 mm ball made from aluminium foil at a depth of 2 cm.

An example of *in vivo* imaging is demonstrated in figure 4. The measurements were made on the breast of a male volunteer, aged 40 years, in good health and of normal body habitus. Many electrodes were in poor contact with the body. The areas of poor contact appear as white fields accompanied with dark artefacts on the periphery of the images. Nevertheless, the central parts of the images, corresponding to three depth levels, appear to demonstrate good correlation with underlying anatomic structures. The nipple area appears to be visible as a highly-conductive area on the most superficial image (figure 4(a)) but has low conductivity in deeper layers (figure 4(b, c)). The ribs become appear to be visible in an image slice 1 cm deep. The muscle tissues appear to be homogeneous in the imaged area.

3. Clinical measurements

21 women with tumours in one breast were examined. The size of tumours, determined by x-ray mammography, was 1.5 to 5 cm. The contralateral breast was assumed to be healthy. Examinations were made in two positions—lying and standing. This resulted in 84 electrical impedance mammograms (EIMs) in total. These were sorted into five groups. (1) 42 EIMs in the normal breast contralateral to that containing the tumour. (2) 42 EIMs in the breast with a clinical diagnosis of breast cancer. Group (2) was subdivided according to whether focal abnormalities could be seen on visual inspection of EIM. (3) 16 EIMs without focal abnormalities. (4) 26 EIMs with such abnormalities. The focal abnormalities in this group were confirmed by x-ray mammography. They appeared on EIT images as white (highly conductive) areas. (5) This group, 13 EIMs, was created by selection of the peak highly conductive areas of group (4). It therefore refers not to whole images, but merely the properties of the most conductive regions in the pathological breasts of patients with cancer. The clinical diagnosis was confirmed by x-ray mammography prior to surgery and histology after surgery and excision of the tumour. The average age of patients was 60 years; 50% of patients had arterial hypertension; 27% had a family history of cancer.

EIM were reconstructed every 8 mm down to a depth of 6 cm (seven scanning planes). Wet gauze was placed between the breast skin and electrode array to improve electric contact. Image acquisition in one patient (preparation, measurements, image reconstruction and processing) took about 15–20 min. The analysis of EIM included (i) visual analysis of images at different depths, (ii) image filtering and calculation of generalized characteristics of conductivity and its variability (average, standard deviation, max and min values) and (iii) presentation of images according to the frequency distribution of conductivity and comparison of the frequency distribution of healthy and ill breast tissues using non-parametric analysis of difference (Kolmogorov–Smirnov criteria).

4. Results

4.1. Breast images

EIM were compared with mammograms obtained from the same scanning plane. With increasing depth, the scanning area of breast decreases, due to limitations in the data. In all images given in this paper, the peripheral area, especially the corners, is the region which has bad contacts, so peripheral dark contours are artefacts which are related to the transition from good to bad contacts. Only the central regions inside these contours are therefore suitable for analysis.

The normal breast image (figure 5) is characterized by an absence of focal abnormalities and has smooth contours of conductivity ('mosaic'). These are seen in scanning planes. Breast cancer EIMs (figure 6) are characterized by focal abnormalities which appear as clear-cut light areas of high conductivity. In the EIM, the focus size varied from 2.0×0.8 cm^2 up to 3.2×3.0 cm^2, spreading to a depth of 3 cm.

4.2. Statistics

During analysis of these EIM images, focal abnormalities in the images, which represent tumours, were seen in 14 of a total of 21 studies, 67%. Another four EIMs without clear abnormalities were nevertheless classified as abnormal due to a conductivity distribution different from the typical distribution in normal breast. As a result, 86% of examinations were

Figure 5. EIM image of intact breast at a depth of 1.2 cm.

Figure 6. EIM image of breast cancer with a 1.2 cm scanning plane; the cancerous area is above and to the left of the centre of the image.

found to be fully or partially consistent with diagnoses made by other independent methods. The causes of data mismatch included (i) enlarged breasts hamper examination due to limited scanning depth, (ii) some BCDD examinations were performed after medical treatments such as puncture, biopsy, or x-ray therapy), which influenced the EIM.

Tissue conductivity was calculated in conventional units. The average conductivity of intact and ill breasts at all scanning planes had a normal distribution. For example, at the most superficial plane, the mean value was $\mu = 0.89$ with a standard deviation $\delta = 0.034$.

Average breast conductivity and standard deviations for groups (1) and (2) at different scanning planes are given in table 1. A systematic decrease of conductivity with depth is observed and may be attributed to the reconstruction software. It should be possible to improve this in the future by choosing more correct weighting coefficients for the back projection procedure. No statistically significant differences in average conductivity between these groups were found.

Table 1. Average breast conductivity i n group (1) and group (2).

	Scanning plane 1 (0.4 cm)	Scanning plane 3 (2.0 cm)	Scanning plane 5 (3.6 cm)
Intact breast	0.89 ± 0.028	0.77 ± 0.056	0.68 ± 0.058
Cancer	0.88 ± 0.042	0.76 ± 0.077	0.69 ± 0.066

Table 2. Average breast conductivity after subdividing of group (2).

	Scanning plane 1 (0.4 cm)	Scanning plane 3 (2.0 cm)	Scanning plane 5 (3.6 cm)
Group 1	0.89 ± 0.028	0.77 ± 0.056	0.68 ± 0.058
Group 3	0.86 ± 0.026	0.72 ± 0.049	0.66 ± 0.053
Group 4	0.91 ± 0.037	0.81 ± 0.066	0.70 ± 0.067
Group 5	0.99 ± 0.038	0.97 ± 0.067	0.96 ± 0.026

Average breast tissue conductivity in groups (3)–(5) is presented in table 2. The averages of groups across scanning planes are significantly different, using variance analysis. With a multiple comparison method—the Newman–Keils criterion (Glantz 1994) we have shown that averages of all groups at scanning planes 1 and 3 significantly differ from each other. At the fifth scanning plane, there was no significant difference.

4.3. Conductivity distribution on EIM

To compare images more accurately, we used histograms of conductivity. To obtain a reference distribution, we built an average histogram of frequency distribution of conductivity for intact breasts (average histogram); it is close to a Gaussian distribution. This was then compared with histograms of each EIM in groups (2), (3) and (4). The histograms were compared qualitatively using such parameters as modality (the number of the local maxima in histograms) and symmetry. In groups (3) and (4), the percentage of multi-modal distributions increased with the increase of scanning depth.

For quantitative estimation of the difference of conductivity distribution between the normal group (1) and the EIMs from groups (3) and (4) (figure 7), we used the concept of the distribution difference value (D_x). The calculation of D_x was carried out through the Kolmogorov–Smirnov algorithm (see, for example, Gubler 1978). According to Gubler, a high significance is observed with distribution difference values of 35–50%. For $D_x = 40\%$, as a criterion of separation of distributions, we found that for group (3) and group (4) 90% of EIM diagrams (19 of 21) have a significant difference from the normal group (1).

5. Discussion

These first experiments have demonstrated that a single frequency static imaging EIT system with 256 electrodes, arranged in a two-dimensional square, is capable of producing images which may be usable in breast cancer detection. The breast is a complex alveolar–tubular gland which consists of 15–20 lobules, encircled by adipose tissue. The complicated anatomical structure of breast tissue may explain the 'mosaic' electrical impedance image of healthy breast. The appearance of focal abnormalities in EIM as clear-cut light areas is due to increases in local conductivity. This has been described for tumours, which are usually vascular. Such focal abnormalities found in 67% of patients with breast cancer.

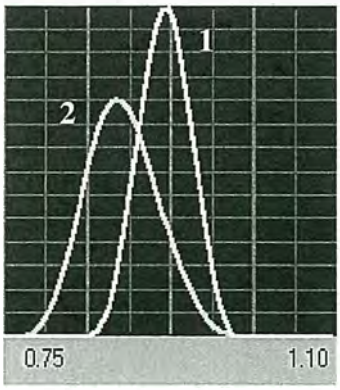

Figure 7. Comparison of EIM histograms: 1—average histogram of normal breast images; 2—one histogram for a breast with cancer; the D_x parameter is 51% for these two distributions.

Analysis of the average conductivity of breast tissues showed that, in groups (1), (3), (4) and (5), it differs significantly at all scanning planes. In the regions estimated solely to correspond to tumour (group (5)) increased conductivity was apparent at all scanning planes. A decrease of average conductivity in breast tissues in group (3) (breasts with tumour but no focal abnormalities on EIM) may be due to changing of electrical characteristics after x-ray medical treatment or a background state preceding the appearance of tumour.

To determine differences in conductivity histograms in groups (1)–(4), it was necessary to use non-parametric criteria. The approach developed in this work for estimating the difference of conductivity histograms, based on the Kolmogorov–Smirnov criterion, may be useable in population screening examinations. Further planned studies will involve a larger number of patients, and will take into account the menstrual cycle, presence of cysts and other benign changes in breast tissue, in order to get more reliable data.

Acknowledgments

This work was supported by Technology Commercialization International, Inc., 1650 University Boulevard, NE, Albuquerque, NM 87102, USA as part of the TC International Breast Cancer Detection Device program.

References

Cherepenin V A, Korjenevsky A V, Kornienko V N, Kultiasov M Y and Kultiasov Y S 1995 The electrical impedance tomograph: new capabilities *Proc. 9th Int. Conf. on Electrical Bio-Impedance (Heidelberg, 1995)* pp 430–33

Glantz S A 1994 *Primer of Biostatistics* (New York: McGraw-Hill)

Gubler E 1978 *Calculation Methods of Analysis and Recognition of Pathological Processes* (Leningrad: Meditsina)

Korjenevsky A V 1995 Reconstruction of absolute conductivity distribution in electrical impedance tomography *Proc. 9th Int. Conf. on Electrical Bio-Impedance (Heidelberg, 1995)* pp 532–5

Korjenevsky A V, Kornienko V N, Kultiasov M Y, Kultiasov Y S and Cherepenin V A 1997 *Prib. Tekh. Exp.* No 3 133-40 (Engl. transl. Korzhenevskii A V, Kornienko V N, Kul'tiasov M Y, Kul'tiasov Y S and Cherepenin V A Electrical impedance computerized tomograph for medical applications *Instrum. Exp. Tech.* **40** 415–21)

Rigaud B, Morucci J P and Chauveau N 1996 Bioelectrical impedance techniques in medicine part I: bioimpedance measurements second section: impedance spectrometry *Crit. Rev. Biomed. Eng.* **24** 257–351

Tunstall B, Wang W, Cheng Z, McCormik M, Walker R and Rew D 1998 *In vitro* study results from De Montfort Mkl electrical impedance mammography system *Proc. 10th Int. Conf. on Electrical Bio-Impedance (Barcelona, 1998)* pp 525–28

Wtorek J, Stelter J and Nowakowski A 1999 Impedance mammograph 3D phantom studies *Ann. NY Acad. Sci.* **873** 520–33